Journal of the Serbian Society for Computational Mechanics / Vol. 19 / No. 1, 2025 / pp 155-166 / review paper
(10.24874/jsscm.2025.19.01.08)

PENALTY CONTACT BETWEEN FEM AND SPH WITH FRICTION

Marko Topalović[1*] [0000-0001-6101-755X], Miloš Ivanović[2] [0000-0002-8974-2267], Snežana Vulović[1] [0000-0001-5784-0906], Aleksandar Nikolić[1] [0000-0002-7052-7444] and Miroslav Živković[3] [0000-0002-0752-6289]

[1] Institute for Information Technologies, University of Kragujevac, Kragujevac, Serbia
e-mail: topalovic@kg.ac.rs, vsneza@kg.ac.rs, dziga@kg.ac.rs
[2] Faculty of Science, University of Kragujevac, Kragujevac, Serbia
e-mail: mivanovic@kg.ac.rs
[3] Faculty of Engineering, University of Kragujevac, Kragujevac, Serbia
e-mail: zile@kg.ac.rs
**corresponding author*

Abstract

The interaction between the Finite Element Method (FEM) and Smoothed Particle Hydrodynamics (SPH) is crucial in multiphysics simulations of granular–structure systems, impacts, and material behavior. This paper presents a penalty-based contact algorithm with Coulomb friction for FEM–SPH coupling. The method accounts for static and dynamic friction and ensures stable force transfer between SPH particles and FEM nodes. A numerical example of granular pile sliding on a steel plate demonstrates the approach. The results confirm that the proposed algorithm provides an efficient and robust framework for FEM–SPH interaction, improving the applicability of SPH in structural, geomechanical, and fluid–structure simulations.

Keywords: Smoothed Particle Hydrodynamics, Finite Element Method, Contact Algorithm, Multiphysics Simulation, PAK (Program za Analizu Konstrukcija)

1. Introduction

The Finite Element Method (Kojić, Slavković, Živković, & Grujović, 1998), with the acronym FEM, which will be used hereinafter, is a numerical method based on the approximation of the real world into a continuum representation (Kojić & Bathe, 2005). FEM can be used for solving problems of solid mechanics (Holzapfel, 2000), and fluid mechanics (Filipovic, Ivanovic, & Kojic, 2009).

Within the PAK-Multiphysics, the PAKS solver is used for solid analysis, while the PAKF solver is used for fluid analysis. Integrating both the fluid and solid solvers into the same executable program and using a parallel programming technique allows for the most efficient FSI simulations (Lv, Zhao, Huang, Xia, & Wang, 2006). This approach was also used in the program PAK-Multiphysics, and in this paper, we will showcase the coupling of PAKS solver used for solids, with MCM (Meshless Continuum Mechanics) solver (De Vuyst, Vignjević, & Campbell, 2005), which is based on SPH (Liu & Liu, 2003). Coupling between PAKS with MCM is very similar to the coupling between PAKS and PAKF because MCM is also written in

FORTRAN. Although PAKF is better suited than MCM for fluid simulation (Topalovic et al., 2022), FSI can also be simulated using PAKS-MCM coupling. However, the main reason for this coupling was the development of a robust solution for modelling of the interaction of granular materials with steel structures.

The rest of the paper is divided into sections in which the coupling of FEM nodes and SPH pseudo-particles is described, with the description of the treatment of friction in contact. Results presented in this paper showcase a simple example of a granular pile placed on a steel plate, which is fixed on one side while the other is lifted until the granular pile slides over and falls off. Finally, the Conclusion section summarizes the presented procedures and outlines future work showcasing the advantages and limitations of the presented methodology.

2. Coupling FEM nodes and SPH pseudo-particles

Modelling the interaction of bodies discretized using FEM and SPH relies on the master/slave principle, in which control is unidirectional i.e. the master controls the slave while the reverse is not possible (De Vuyst, Vignjević, & Campbell, 2005). In the case of coupling FEM and SPH programs, the FEM program plays the role of master while the SPH program is the slave. This coupling method allows for the analysis of fluid-solid interaction as well as the modeling of ballistic impact and penetration. (De Vuyst, Vignjević, & Campbell, 2005). The original implementation of the master/slave principle was based on the predictor-corrector algorithm, in which the positions of the master surfaces and slave pseudo-particles were calculated in the predictor phase as if there was no contact, and then the penetration depth of the slave pseudo-particles into the master surface was calculated in the corrector phase (Attaway, Heinstein, & Swegle, 1994). Based on the calculated penetration, the contact force acting on the master surface and the slave pseudo-particle is calculated, which separates the contact in the next time step.

The master/slave algorithms used to connect SPH and FEM are based on two approaches: the attached particle approach and the sliding contact approach (Johnson, 1994). In the first approach, the nodes of the elements participating in the contact also represent the contact layer of SPH particles, as can be seen from Fig. 1.

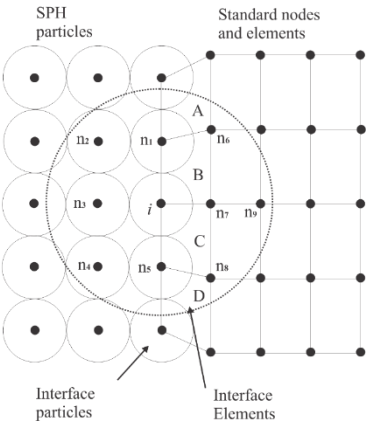

Fig. 1. SPH attachment to FEM according to Johnson (1994)

The size of the contact particles corresponds to the size of the contact elements as can be seen from Fig. 1. The mass of the contact particles originates exclusively from the material modeled by SPH particles, so the mass of all contact particles is the same (Johnson, 1994). For the observed particle i, the influence domain is represented by a dashed line, as can be seen from Fig. 1. Although in the given influence domain, in addition to SPH particles, there are also standard FEM nodes, the deformations and deformation rates are calculated only based on the common nodes. The forces in the particle i originate from these nodes and elements B and C, while the standard FEM nodes do not participate directly, but through elements B and C.

The sliding contact approach implies that the SPH particles and the FEM nodes are not rigidly connected, but rather contact is established between the SPH particles and the edges/faces of the finite elements as can be seen from Fig. 2.

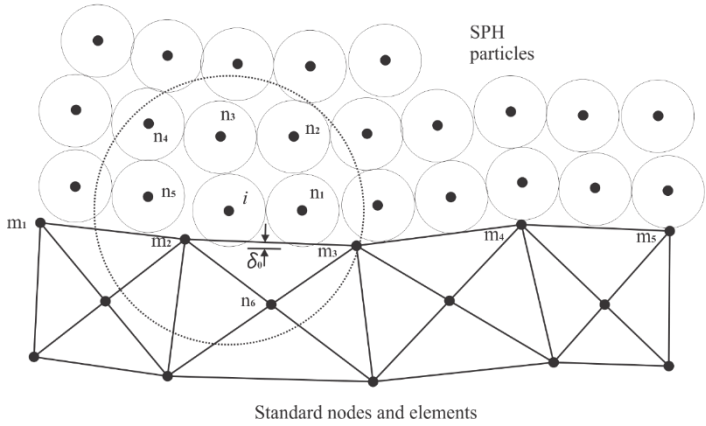

Fig. 2. Sliding contact approach according to Johnson (1994)

Similar to the case of attached particles, in the case of sliding contact, standard FEM nodes m_2, m_3, n_6 do not participate in the calculation of deformations, deformation rates and forces in the observed SPH particle *i* (Johnson, 1994). The maximum allowed overlap of the slave SPH particle *i* with the host FEM surface $m_2 - m_3$ is denoted by δ_0 and in the case of classically generated SPH particles it is equal to zero, while in the case of SPH particles obtained by erosion of FEM elements, it can have a small value representing a fraction of the interparticle distance (Johnson & Stryk, 2003). If there is a partial overlap of the slave particle *i* with the master segment $m_2 - m_3$ which is denoted as $(\delta > \delta_0)$, the normal velocities of particle *i* and nodes m_2 and m_3 must be updated so that the law of conservation of momentum holds and the normal velocity of particle *i* corresponds to the velocity of the segment $m_2 - m_3$.

The sliding contact approach implies that the SPH particles and the FEM nodes are not rigidly connected, but rather contact is established between the SPH particles and the edges/faces of the finite elements as can be seen from Fig. 2.

In addition to the aforementioned interfaces with attached particles and with sliding contact (which arise from connecting SPH with FEM), boundary SPH particles can be on a free surface, in contact with another material, they can be assigned essential (geometric) boundary conditions (displacement) or natural boundary conditions (forces or stresses) as can be seen from Fig. 3.

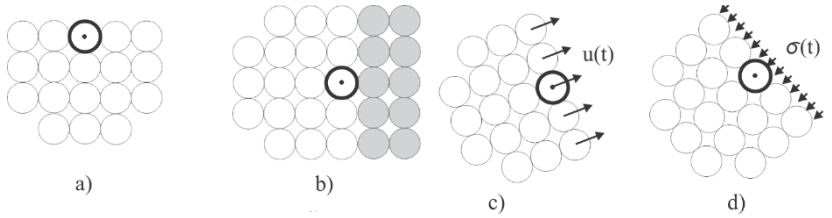

Fig. 3. Possible boundaries of SPH particle (Johnson 1994): a) free surface, b) contact with another material, c) geometric boundary conditions, d) natural boundary conditions

In the case of a free surface, the boundary layer of particles has an incomplete set of neighboring particles (since the boundary surface intersects the influence domain), so if one wants to avoid this drawback, it is possible to add virtual particles. If two different materials are in contact, an error occurs in the calculation of the rate of change of deformation and the rotation tensor, because when summing over all neighboring particles, particles of different materials with different material characteristics enter the sum (Johnson, Beissel, & Stryk, 2002). The smaller the difference in material characteristics, the smaller the error, so if the contact of two bodies made of the same material is modeled, there is no error in the contact layers. In the case of different materials, it comes from some penetration and mixing at the contact surface, since SPH does not need that the velocity field has a unique value (Campbell, Vignjević, & Libersky, 2000). The solution was to introduce a penalty force within the pinball algorithm (Belytschko & Yeh, 1993), which acts between particles in contact and whose intensity depends on the overlap and the rate of change of the overlap, and which is calculated based on the following expressions:

$$p = \frac{h_i + h_j}{2} - \left| x_j - x_i \right| \geq 0 , \tag{1}$$

$$F = K_p \min\left(F_1, F_2\right), \tag{2}$$

$$F_1 = \begin{cases} \dfrac{\rho_i \rho_j R_i^3 R_j^3}{\rho_i R_i^3 + \rho_j R_j^3} \cdot \dfrac{\dot{p}}{\Delta t} & \dot{p} > 0 \\ 0 & \dot{p} < 0 \end{cases}, \tag{3}$$

$$F_2 = \left[\frac{G_i G_j}{G_i + G_j} \sqrt{\frac{R_i R_j}{R_i + R_j}} \right] p^{3/2} . \tag{4}$$

In the previous expressions, for particles in contact defined by coordinates x_i and x_j, the smoothing lengths are denoted by h_i and h_j, their overlap is denoted by p, while ρ_i and ρ_j are their densities, R_i and R_j are their radii, with G_i and G_j representing the shear moduli for the given materials (Belytschko & Yeh, 1993). The force calculated in this way can be corrected by a certain scaling factor K_p (Campbell, Vignjević, & Libersky, 2000).

The contact between two different materials in the SPH method can be viewed as contact between a particle and a surface, or as contact between particles, as can be seen from Fig. 4.

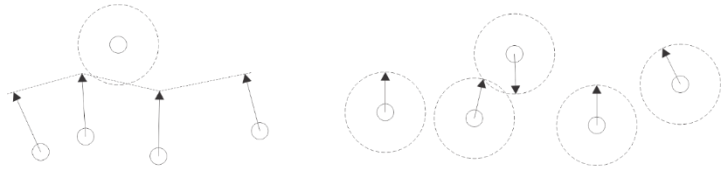

Fig. 4. Contact determination: (a) Particle and surface; (b) Contact between particles.

Contact between particles is more convenient for application and is more consistent with the meshless character of the SPH method, but there is an issue with determining the direction of action of the contact force since normals in the contacting particles do not generally coincide (Campbell, Vignjević, & Libersky, 2000). If the contact forces are defined along the vector connecting the centers of the particles in contact (as is the case with the pinball algorithm), the contact forces have a normal and a tangent component. If it is necessary to avoid the tangent component of the contact forces, it is necessary to calculate the average normal between the particles and define the contact forces along it (Campbell, Vignjević, & Libersky, 2000). After the pinball algorithm (Belytschko & Yeh, 1993), more complex algorithms for the calculation of penalty force were developed (Campbell, Vignjević, & Libersky, 2000) among which is the contact potential algorithm which will be modified and used in this paper (De Vuyst, Vignjević, & Campbell, 2005). The contact potential algorithm is based on Monaghan's idea of introducing a repulsive term Rf_n^{ij} to mitigate tension instability into an expression for the law of conservation of momentum (Monaghan, 2000), which now reads:

$$\frac{Dv_\alpha^i}{Dt} = -\sum_{j\in SS} m^j \left(\frac{\sigma_{\alpha\beta}^j}{\rho^{j2}} + \frac{\sigma_{\alpha\beta}^i}{\rho^{i2}} + Rf_n^{ij} \right) \frac{\partial W^{ij}}{\partial x_\beta^i}, \tag{5}$$

where R is the coefficient that depends on pressure and density, and the repulsive force f_n^{ij} is given with:

$$f_n^{ij} = \frac{W\left(r^{ij}\right)}{W\left(\Delta p_{avg}\right)}, \tag{6}$$

where $r^{ij} = \left|\mathbf{x}^i - \mathbf{x}^j\right|$ is the distance between particles *i* and *j*, while Δp_{avg} is the average interparticle distance in the vicinity of the observed particle *i*. As the distance r^{ij} decreases, the repulsive force increases (Monaghan, 2000).

The contact potential is given by the expression:

$$\phi\left(\mathbf{x}^i\right) = \int_{\Omega_c} K \left(\frac{W\left(\mathbf{x}^i - \mathbf{x}\right)}{W\left(\Delta p_{avg}\right)} \right)^n dV, \tag{7}$$

where Ω_c represents the intersection of the influence domain of the observed particle and the neighboring body with which the observed particle is in contact, while K and n are user-defined parameters that regulate the intensity of the potential (De Vuyst, Vignjević, &

Campbell, 2005). Based on equation (7), it can be concluded that the value of the contact potential is always greater than or equal to zero within the domain to which the contacting particle belongs and that, similarly to Monaghan's repulsive force (6), it increases as the distance between the particles in contact decreases (De Vuyst, Vignjević, & Campbell, 2005). Using the particle approximation, the expression for the contact potential (7) becomes:

$$\phi\left(\mathbf{x}^i\right) = \sum_j^{NCONT} \frac{m^j}{\rho^j} K \left(\frac{W\left(\mathbf{x}^i - \mathbf{x}^j\right)}{W\left(\Delta p_{avg}\right)} \right)^n \tag{8}$$

Volume force $b_c\left(\mathbf{x}^i\right)$ is calculated as the contact potential gradient (De Vuyst, Vignjević, & Campbell, 2005):

$$b_c\left(\mathbf{x}^i\right) = \nabla\phi\left(\mathbf{x}^i\right) = \sum_j^{NCONT} \frac{m^j}{\rho^j} K \frac{W\left(\mathbf{x}^i - \mathbf{x}^j\right)^{n-1}}{W\left(\Delta p_{avg}\right)^n} \nabla_{x_i} W\left(\mathbf{x}^i - \mathbf{x}^j\right) \tag{9}$$

The contact force vector $f_c\left(\mathbf{x}^i\right)$ is obtained by integrating the volume force vector $b_c\left(\mathbf{x}^i\right)$:

$$f_c\left(\mathbf{x}^i\right) = \int_{\Omega_c} \mathbf{N}^T b_c\left(\mathbf{x}^i\right) dV \tag{10}$$

where $\mathbf{N}$ is a normalized matrix of weighting or interpolation functions, whose members are:

$$N_{ij} = \frac{m^j}{\rho^j} \frac{W\left(\mathbf{x}^i - \mathbf{x}^j\right)}{\sum_{j \in SS} \frac{m^j}{\rho^j} W\left(\mathbf{x}^i - \mathbf{x}^j\right)} = \frac{m^j}{\rho^j} \tilde{W}\left(\mathbf{x}^i - \mathbf{x}^j\right) \tag{11}$$

where SS is a set of neighboring particles, the normalized kernel is denoted by $\tilde{W}\left(\mathbf{x}^i - \mathbf{x}^j\right)$.

Substituting (11) and (9) in (10), after integration, taking into account that the member $\frac{m^i}{\rho^i}$ constant and based on the conditions of division of the unity (Liu & Liu, 2003), we obtain the final form of the expression for the contact force vector:

$$f_c\left(\mathbf{x}^i\right) = \sum_j^{NCONT} \frac{m^j}{\rho^j} \frac{m^i}{\rho^i} K \frac{W\left(\mathbf{x}^i - \mathbf{x}^j\right)^{n-1}}{W\left(\Delta p_{avg}\right)^n} \nabla_{x_i} W\left(\mathbf{x}^i - \mathbf{x}^j\right) \tag{12}$$

When the acceleration due to the contact force $\frac{f_c\left(\mathbf{x}^i\right)}{m^i}$ is added to the (12) the final form of the momentum balance law for the contact potential algorithm is obtained (De Vuyst, Vignjević, & Campbell, 2005):

$$\frac{Dv_\alpha^i}{Dt} = -\sum_{j\in SS} m^j \left(\frac{\sigma_{\alpha\beta}^j}{\rho^{j2}} + \frac{\sigma_{\alpha\beta}^i}{\rho^{i2}} \right) \frac{\partial W^{ij}}{\partial x_\beta^i} - \frac{f_c\left(\mathbf{x}^i\right)}{m^i} \tag{13}$$

3. Treatment of friction contact

Whether the contact between materials in the SPH method is modeled using the contact potential algorithm, or by including particles of both materials in the summation within the influence domain *2h*, friction as a fundamental characteristic of granular materials has not been given adequate attention. In order to model the interaction of granular materials with devices for their transport, processing and storage, which is based on the connection of FEM with SPH, a few important assumptions should be highlighted:

- FEM shell elements are used to model the aforementioned devices, which are characterized by the property that one dimension is significantly smaller than the other two. When connecting the FEM and SPH methods, SPH particles are generated from the nodes of these elements. Unlike the original fixed particle approach from Fig. 1. in which all SPH particles (including contact ones) are made of the same material, in this case, the particles generated from the FEM nodes are assigned the material characteristics of the corresponding elements.

- The displacements of the nodes are calculated in FEM, while the corresponding generated SPH particles are fixed during the SPH calculation. The forces acting on the generated contact particles are transferred from SPH to FEM (according to the same principle as the fluid-structure interaction in FEM), where the displacements and stresses are calculated based on them.

- The contact forces are decomposed into normal and tangential components, after which the friction condition is checked, i.e. whether the friction is static or dynamic. In the case of static friction, there is no sliding of the granular material on the contact surface, while in the case of dynamic friction, there is sliding, and the friction force opposes this sliding.

Since the contact surface may be irregularly shaped, it is first necessary to find the normal to the contact surface in the observed particle *i*. Whether a particle belongs to the boundary layer can be determined by performing a kernel approximation of some characteristic "color" scalar function ψ (Randles & Libersky, 1996) so that for the boundary particle *i* it holds:

$$\psi^i \neq \sum_{j\in SS} \psi^j \frac{m^j}{\rho^j} W\left(\mathbf{x}^i - \mathbf{x}^j\right), \tag{14}$$

since in summation over all neighboring particles SS, particles of "other colors" are also included.

The material identification is used as the "color" function. Determining the normal based on the "color" function was originally used in FEM analysis of the contact of two fluids in the *Euler* spatial formulation (Brackbill, Kothe, & Zemach, 1992). Subsequently, *Randles* and *Libersky* applied this principle in the SPH method (Randles & Libersky, 1996). A schematic representation of two fluids in contact can be seen in Fig. 5.

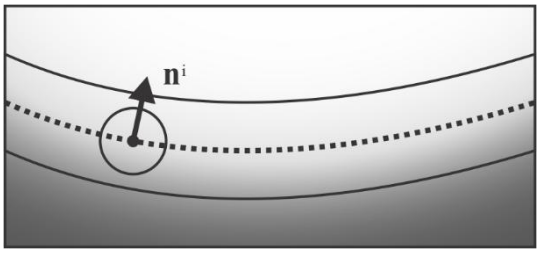

Fig. 5. Normal to the contact surface at point i

Here, computational details are given, following (Randles & Libersky, 1996). The normal in the observed contact particle is calculated based on the following expression:

$$\mathbf{n}^i = \pm \nabla \psi^i \tag{15}$$

where

$$\nabla \psi^i \neq \sum_{j \in SS} \psi^j \frac{m^j}{\rho^j} \nabla W\left(\mathbf{x}^i - \mathbf{x}^j\right) \tag{16}$$

The sign in equation (15) is always minus if all neighboring particles are of the same material as the observed particle *i* (Randles & Libersky, 1996).

After determining the normal, it is possible to decompose the contact force given by expression (11) into a normal and tangential component as can be seen from Fig. 6.

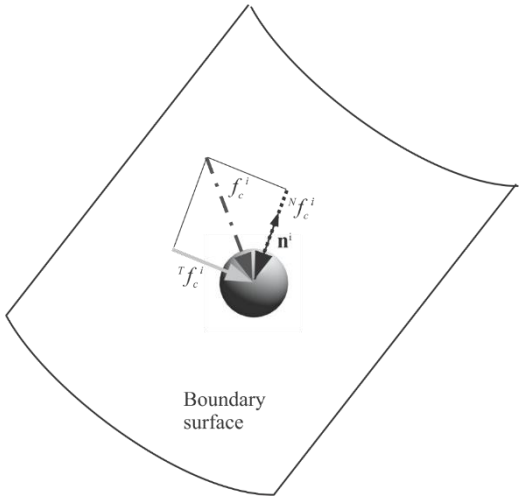

Fig. 6. Components of the contact force in a boundary particle

The normal component is a projection of a vector based on the following expression:

$$^N\mathbf{f}_c^i = \frac{\mathbf{f}_c^i \cdot \mathbf{n}^i}{\left|\mathbf{n}^i\right|} \frac{\mathbf{n}^i}{\left|\mathbf{n}^i\right|}, \tag{17}$$

while the tangent component is given by the equation:

$$ {}^{T}\mathbf{f}_c^i = \mathbf{f}_c^i - {}^{N}\mathbf{f}_c^i \tag{18} $$

Now it is necessary to check whether it is static or dynamic friction based on *Coulomb's* law of friction. In the case of static friction, there is no movement between the contacting surfaces, because the intensity of the tangential component of the contact force is less than the critical value, which is mathematically represented by the inequality:

$$ \mathbf{f}_{fs}^i = -{}^{T}\mathbf{f}_c^i \le \mu_s {}^{N}\mathbf{f}_c^i, \tag{19} $$

where μ_s represents the static coefficient of friction.

In the case of static friction, the friction force $\mathbf{f}_{fs}^i$ is of the same intensity and opposite direction to the tangential component of the contact force ${}^{T}\mathbf{f}_c^i$ and can have a value between 0 and $\mu_s {}^{N}\mathbf{f}_c^i$. If the tangent component ${}^{T}\mathbf{f}_c^i$ is greater than $\mu_s {}^{N}\mathbf{f}_c^i$, there is movement between the contact surfaces, and the sliding friction force is given by:

$$ \mathbf{f}_{fk}^i = \le \mu_k {}^{N}\mathbf{f}_c^i, \tag{20} $$

where $\mu_k \le \mu_s$ represents the kinematic coefficient of friction.

Regardless of whether it is static or dynamic friction, the expression for the law of conservation of momentum is given by the expression (13) should be corrected by including the friction force:

$$ \frac{Dv_\alpha^i}{Dt} = -\sum_{j\in SS} m^j \left(\frac{\sigma_{\alpha\beta}^j}{\rho^{j2}} + \frac{\sigma_{\alpha\beta}^i}{\rho^{i2}} \right) \frac{\partial W^{ij}}{\partial x_\beta^i} - \frac{f_c\left(\mathbf{x}^i\right)}{m^i} - \frac{f_{f\alpha}^i}{m^i} \tag{21} $$

where the friction force f_f^i can be static or dynamic based on condition (20)

$$ f_{f\alpha}^i = \begin{cases} f_{fs\alpha}^i = -{}^{T} f_c^i & {}^{T}\mathbf{f}_c^i \le \mu_s {}^{N}\mathbf{f}_c^i \\ f_{fk\alpha}^i = -\mu_k {}^{N} f_c^i & {}^{T}\mathbf{f}_c^i > \mu_s {}^{N}\mathbf{f}_c^i \end{cases} \tag{22} $$

4. Results

Adequate modeling of the interactions of granular materials with devices used for their storage, transport, and processing requires a combination of FEM and SPH methods, where the granular material is modeled by SPH particles, while the elastoplastic material, from which these devices are made, is modeled by finite elements. This combination adds complexity to multiphysics simulations, representing a significant improvement over the prescription of analytically calculated forces as loads at nodes (Petrović et al., 2015).

In the test example, a gravel cone with a diameter of 123 mm and a height of 27.5 mm was modeled with 478 SPH particles. The plate was modeled with 289 elements and 324 nodes that are copied into an additional 324 SPH particles during the calculation. The maximum displacement at the edge of the plate is 50 mm. Schematic representation of the tipping model can be seen in Fig. 7.

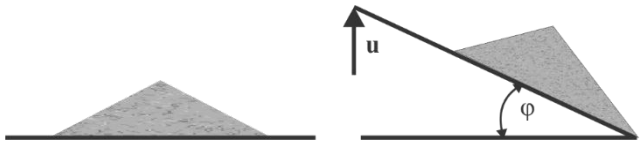

Fig. 7. Components of the contact force in a boundary particle

The cone angle is slightly smaller than the angle of internal friction. The initial state of the model can be seen from Fig. 8**.**

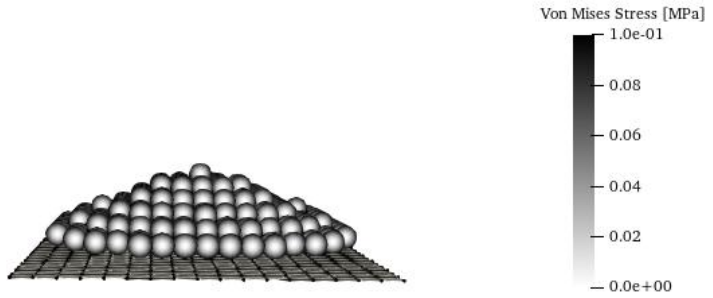

Fig. 8. Components of the contact force in a boundary particle

When the plate is at an angle equal to the angle of internal friction, the entire cone begins to slide along the plate as can be seen from Fig. 9.

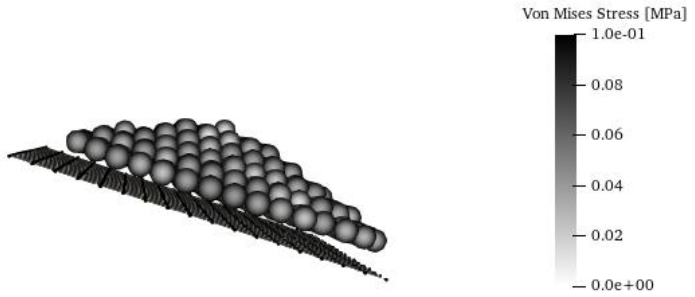

Fig. 9. Components of the contact force in a boundary particle

This time period is characterized by a transition from static to kinematic friction previously described by Eq. (20). Sliding and stretching continue and accelerate with increasing plate angle, and at time t=0.5s, the plate motion stops. After 0.6s, a significant portion of the granular material is in a state of free fall, and the remainder of the cone is located near the fixed edge of the plate, as can be seen from Fig. 10.

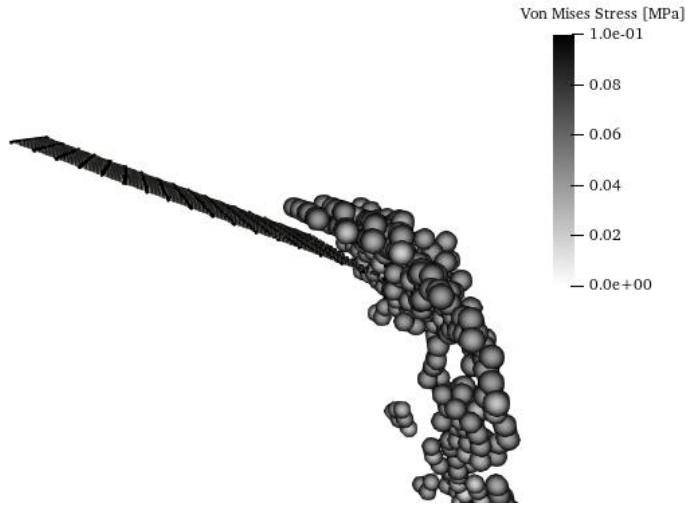

Fig. 10. Components of the contact force in a boundary particle

5. Conclusions

The tipping of a cone made of granular material demonstrated that the proposed FEM–SPH coupling can reproduce realistic granular behavior. However, all FEM nodes need to be copied into SPH, and contact is calculated exclusively in the MCM solver, which increases computational cost. Our future work will focus on a more efficient solution that will involve generating a reduced list of contact nodes within the PAK input file, which would be later transferred to MCM. Further progress also requires implementation of the sliding contact approach, which would broaden the applicability of the framework within various multiphysics fields.

The showcased methodology is simple to implement because PAK already supports nodal force transfer, and MCM includes contact handling. Also, the presented penalty-based algorithm is enhanced with static and dynamic Coulomb friction, a critical factor in capturing granular flow, shear resistance, and energy dissipation. The approach is therefore well-suited for multiphysics simulations such as granular transport, soil–structure interaction, and impact dynamics.

Acknowledgements: This research was supported by the Ministry of Science, Technological Development and Innovation of the Republic of Serbia, contract No. 451-03-66/2024-03/200378, and by the Science Fund of the Republic of Serbia, #GRANT No. 7475, Prediction of damage evolution in engineering structures – PROMINENT.

References

Attaway, S. W., Heinstein, M. W., & Swegle, J. W. (1994). Coupling of smooth particle hydrodynamics with the finite element method. Nuclear Engineering and Design, 150(2–3), 199–205. https://doi.org/10.1016/0029-5493(94)90018-9

Belytschko, T., & Yeh, I. S. (1993). The splitting pinball method for contact-impact problems. Computer Methods in Applied Mechanics and Engineering, 105(3), 375–393. https://doi.org/10.1016/0045-7825(93)90068-L

Brackbill, J. U., Kothe, D. B., & Zemach, C. (1992). A continuum method for modeling surface tension. Journal of Computational Physics, 100(2), 335–354. https://doi.org/10.1016/0021-9991(92)90240-Y

Campbell, J., Vignjević, R., & Libersky, L. (2000). A contact algorithm for smoothed particle hydrodynamics. Computer Methods in Applied Mechanics and Engineering, 184(1), 49–65. https://doi.org/10.1016/S0045-7825(99)00228-5

De Vuyst, T., Vignjević, R., & Campbell, J. C. (2005). Coupling between meshless and finite element methods. International Journal of Impact Engineering, 31(8), 1054–1064. https://doi.org/10.1016/j.ijimpeng.2004.06.012

Filipovic, N., Ivanovic, M., & Kojic, M. (2009). A comparative numerical study between dissipative particle dynamics and smoothed particle hydrodynamics when applied to simple unsteady flows in microfluidics. Microfluidics and Nanofluidics, 7, 227–235. https://doi.org/10.1007/s10404-008-0382-z

Holzapfel, G. A. (2000). Nonlinear solid mechanics: A continuum approach for engineering. John Wiley & Sons.

Johnson, G. R. (1994). Linking of Lagrangian particle methods to standard finite element methods for high velocity impact computations. Nuclear Engineering and Design, 150(2–3), 265–274. https://doi.org/10.1016/0029-5493(94)90024-3

Johnson, G. R., & Stryk, R. A. (2003). Conversion of 3D distorted elements into meshless particles during dynamic deformation. International Journal of Impact Engineering, 28(9), 947–966. https://doi.org/10.1016/S0734-743X(02)00083-2

Johnson, G. R., Beissel, S. R., & Stryk, R. A. (2002). An improved generalized particle algorithm that includes boundaries and interfaces. International Journal for Numerical Methods in Engineering, 53(4), 875–904. https://doi.org/10.1002/nme.310

Kojić, M., & Bathe, K.-J. (2005). Inelastic analysis of solids and structures. Springer-Verlag.

Kojić, M., Slavković, R., Živković, M., & Grujović, N. (1998). Metod konačnih elemenata I, Linearna analiza [Finite element method I, Linear analysis]. Faculty of Engineering, University of Kragujevac.

Liu, G. R., & Liu, M. B. (2003). Smoothed particle hydrodynamics: A meshfree particle method. World Scientific Publishing.

Lv, X., Zhao, Y., Huang, X. Y., Xia, G. H., & Wang, Z. J. (2006). An efficient parallel/unstructured-multigrid preconditioned implicit method for simulating 3D unsteady compressible flows with moving objects. Journal of Computational Physics, 215(2), 661–690. https://doi.org/10.1016/j.jcp.2005.11.012

Monaghan, J. J. (2000). SPH without a tensile instability. Journal of Computational Physics, 159(2), 290–311. https://doi.org/10.1006/jcph.2000.6439

Petrović, R., Živković, M., Topalović, M., & Slavković, R. (2015). Analytical, numerical and experimental stress assessment of the spherical tank with large volume. Tehnički Vjesnik, 22(5), 1135–1140. https://doi.org/10.17559/TV-20140220121752

Randles, P. W., & Libersky, L. D. (1996). Smoothed particle hydrodynamics: Some recent improvements and applications. Computer Methods in Applied Mechanics and Engineering, 139(1–4), 375–408. https://doi.org/10.1016/S0045-7825(96)01090-0

Topalovic, M., Nikolic, A., Milovanovic, V., Vulovic, S., & Ivanovic, M. (2022). Smoothed particle hydrodynamics for blood flow analysis: Development of particle lifecycle algorithm. Computational Particle Mechanics, 9, 1119–1135. https://doi.org/10.1007/s40571-022-00465-9